


Click dechlorination of halogen-containing hazardous plastics towards recyclable vitrimers

Received: 1 June 2024

Xiaoyan Qiu¹, Jize Liu¹, Xinkai Li¹, Yuyan Wang² & Xinxing Zhang¹  

Accepted: 29 October 2024

Published online: 11 November 2024

 Check for updates

Amid the ongoing Global Plastics Treaty, high-quality circulation of halogen-containing plastics in an environmentally sound manner is a globally pressing issue. Current chemical dechlorination methods are limited by their inability to recycle PVC at the long-chain carbon level and the persistence of eco-toxic organochlorine byproducts. Herein, we propose a click dechlorination strategy for transforming waste PVC into valuable vitrimers via a one-step cascade thiol-ene click reaction and dynamic polymerization. Thermal activation of C-Cl bonds initiates β -elimination dechlorination, while disulfide bonds synchronously undergo homolytic cleavage, generating sulfur-centered radicals that drive precise sulfur-chlorine substitution and the formation of disulfide dynamic networks. This strategy achieves nearly complete chlorine extraction (93.88%) and produces vitrimers with tailorable mechanical and reprocessing properties, spanning from soft elastomers with 784% elongation to rigid plastics with a yield strength of 34 MPa. The significant advantage of this strategy is backbone protective precise dechlorination, enabling ecosystem toxicity reduced by 99.51% compared with widely adopted pyrolysis methods. This work introduces a sustainable pathway for upcycling PVC into valuable materials, marking significant progress in chlorinated plastic recycling.

Plastic pollution is one of the urgent environmental problems that is currently attracting global attention^{1–3}. Global Plastics Treaty advocates eliminating plastic pollution by promoting higher recycling rates and reducing the emissions of hazardous substances throughout plastics' life cycle^{4,5}. Among these commodity waste plastics, halogen-containing plastics represented by polyvinyl chloride (PVC) are recognized as the most hazardous polymers, which have a high production rate up to 58.9 million metric tons in 2023 but the lowest recycling rate in most countries (less than 0.05 percent in the US, Fig. 1a)⁶. Traditional hydrothermal, hydrogenolysis, pyrolysis, and catalytic cracking methods can't satisfy demands of harmless disposal of waste PVC, due to the uncontrollable Cl radical formation at elevated temperatures causing significant dose release of harmful chlorine-containing organics such as dioxins or corrosive HCl (Fig. 1b)^{7,8}. To address the globally intractable challenge, developing

transformative PVC dechlorination recycling strategies toward sustainability is urgently needed.

Selective removal and stabilization of Cl from the C-C main chain is critical for the harmless treatment of PVC, having attracted increasing research concerns. Recently, some new dechlorination strategies have been explored^{9–11}. For example, Anne et al. reported the electro-reduction method based on paired-electrolysis reactions to remove Cl, which was directly reutilized as chloride sources to synthesize small-molecule chloroarenes¹². Ma et al. proposed a co-upcycling method of PVC and polyesters that, in situ, uses Cl ions to attack the C_{alkyl}-O bonds on the main chain of polyesters, generating 1,2-dichloroethane monomers¹³. Despite a big breakthrough, the footprint of chloride elements is substantially prolonged due to organochlorine yields that potentially cause environmental risks. Besides, nearly all closed-loop chemical recycling methods of

¹State Key Laboratory of Polymer Materials Engineering, Polymer Research Institute, Sichuan University, Chengdu, China. ²Max Planck Institute for Polymer Research, Mainz, Germany. ✉ e-mail: xxzwwh@scu.edu.cn

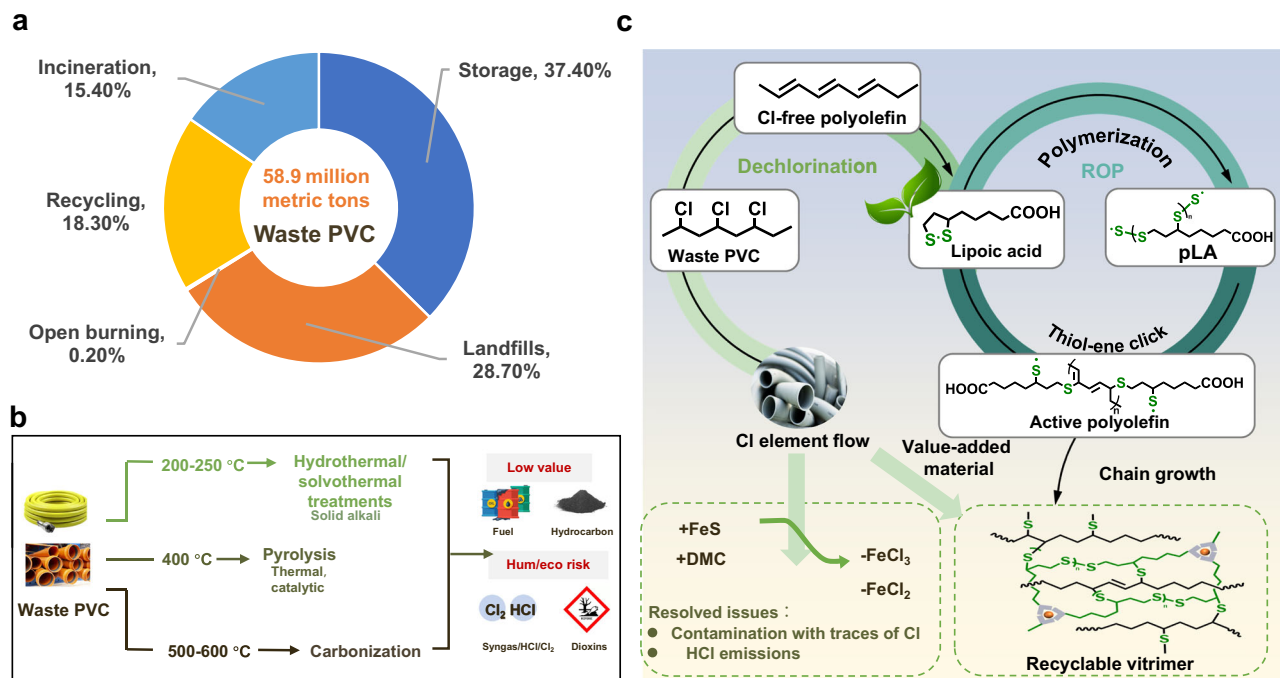


Fig. 1 | Overview of the recycling of PVC wastes. **a** Waste PVC recycling and treatment methods, estimated based on the reuse and recycling of PVC plastics, and global polymer demand in 2016–2050⁶. **b** Current schemes of traditional thermochemical recycling. **c** Cascade reaction routine for transforming PVC into

vitrimer, including three reactions: thermal dechlorination of PVC, ROP of lipoic acid, and thiol-ene click addition reaction between dechlorinated PVC and the thiol of the poly lipoic acid.

depolymerization back to small-molecule are not yet economical because of the maximal number of chemical bonds broken and also constrained by the use of catalysts, complex purification, and long repolymerization routines^{14–17}. Thus, time- and material-efficient methods are immensely sought to convert PVC into bulk materials, preferably without additional separation.

A major challenge in achieving high-quality recycling of PVC is developing a synchronous polymerization method that prevents undesirable polyolefin random cracking and aromatization. The rapid development of click and dynamic chemistries, particularly thiol-ene click reaction, presents a valuable opportunity, showing the advantages of efficiency and mild reaction conditions and being widely used in polymer synthesis, functionalization, and bioengineering^{18–22}. The allyl carbon radicals generated during the pre-dechlorination stage are active reaction sites, enabling the polyene-type macromolecule backbone to be further extended by radical reactions. Integrating thiol-ene click chemistry with dynamic covalent polymer networks enables the creation of vitrimers, materials that combine the recyclability of thermoplastics with the stability of thermosets through reversible cross-linking, facilitating reshaping, repair, and recycling while retaining mechanical properties. However, applying this chemical scheme to PVC for efficient dechlorination and a one-pot transformation remains largely underexplored.

Here, a thiol-ene click reaction coupled with dynamic polymerization was reported, achieving precise sulfur-chlorine substitution for one-step transforming waste PVC into recyclable vitrimers. Click bonding of controllable dechlorination sites and thiol groups cascade with the dynamic ring-opening polymerization (ROP) of the disulfide ring on lipoic acid, which upgrows linear chains into networks (Fig. 1c). This reaction shows a mainchain protection advantage due to the introduction of weak disulfide bonds, that inhibit the PVC chain from degrading to small molecules to achieve macromolecular-state recycling. More importantly, the vitrimers were endowed with added value, showing re-processability and highly tunable mechanical properties. Besides, by efficiently

separating and stabilizing organochlorines, this work dramatically reduces eco/human toxicity compared to the pyrolysis method. This readily adaptable recycling strategy potentially addresses the pressing challenges of waste halogen-containing plastics regeneration, we foresee it will fulfill the intertwined environmental-chemical-material needs in waste plastics circulation.

Results

Sulfur-chlorine substitution mechanistic investigations

The sulfur-chlorine substitution reactions were performed using PVC powder ($M_n = 75968$ g/mol) as the substrate, biologically sourced lipoic acid (LA) as a sulfur source, and synthesized FeS nanoparticles as an efficient trap for Cl ions as it also has a reducibility for C-Cl bonds. These reactions were carried out under one-pot hydrothermal conditions at 150 °C for varying durations. The bond dissociation enthalpy (BDE) of C-Cl (78.57 kcal/mol) and S-S bonds (60.52 kcal/mol) is below that of C-C (85.92 kcal/mol, Fig. 2a), confirmed using density functional theory (DFT), indicating the breakages of disulfide bonds of LA and C-Cl bonds of PVC are preferential to backbone degradation. The 5,5-dimethyl-1-pyrroline N-oxide (DMPO)-trapped electron spin-paramagnetic resonance (EPR) experiments characterized the free radicals in the reactive system were generated²³. A superposition signal of individual free radicals ($g = 2.013, 2.0043$) in the EPR spectrum was captured as temperature increased to 140 °C (Fig. 2b), corresponding to sulfur radicals, and allyl radicals arising from Cl removing, respectively²⁴. EPR results verified the reaction following a free radical mechanism. The observed acidification of the reaction medium suggests that H is also released from the PVC to form HCl, indicating an elimination dechlorination mechanism. While the FeS reactant could neutralize the solution's acidity, as indicated by the pH measurements (Supplementary Fig. 1). ¹H NMR spectroscopy (Fig. 2c) reveals a significant reduction in the characteristic peaks corresponding to the α/β -hydrogens of PVC, observed in the 2.0–2.7 ppm and 4.0–5.0 ppm regions. Concurrently, new resonances emerge at 2.85 ppm, which are attributable to the formation of thiolated PVC. The characteristic peaks

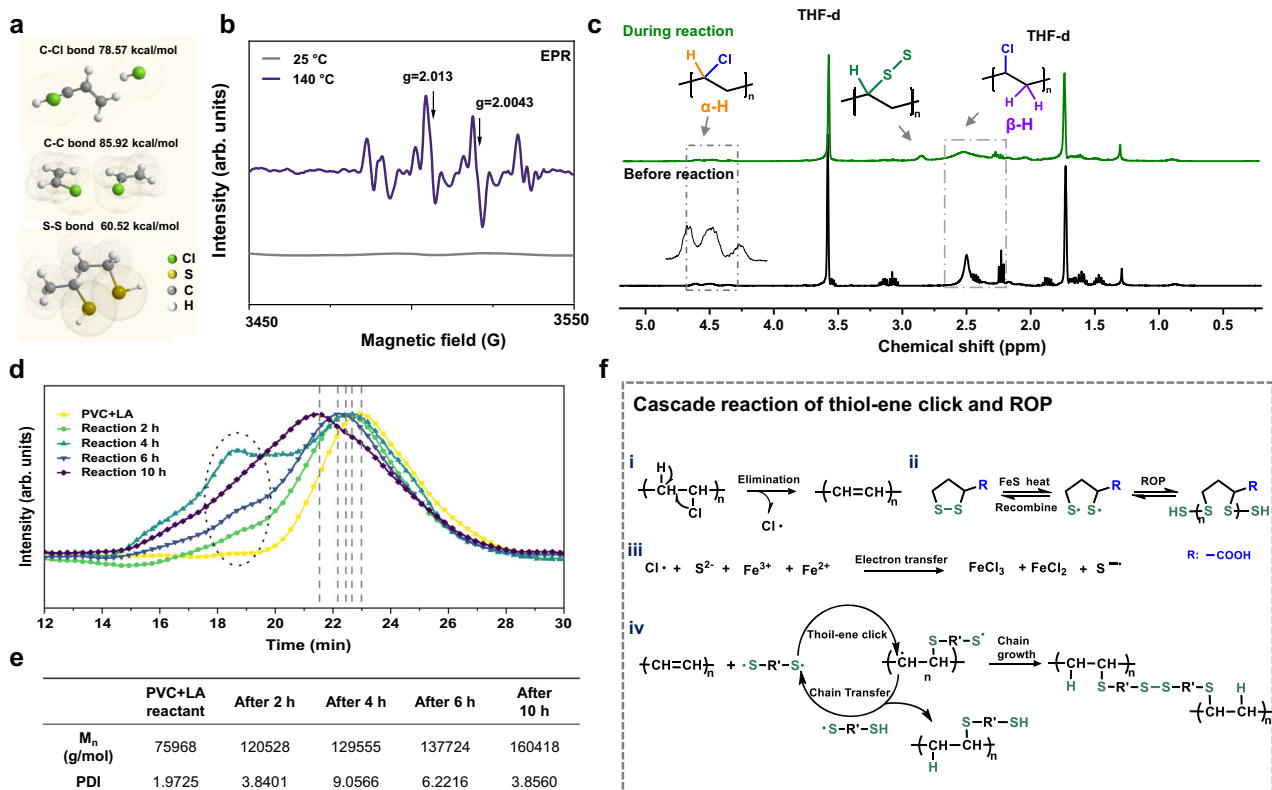


Fig. 2 | Chemical dechlorination recycling pathway for PVC. a BDE of PVC and LA molecular fragments. **b** EPR spectra of the reaction system with radical scavenger DMPO obtained in situ and upon continuous heating. **c** ^1H NMR spectra (400 MHz, tetrahydrofuran-d) of reaction mixture before and during the reaction.

d GPC chromatograms during the reaction. **e** Average molecular weight and polydispersity index during the reaction. **f** Proposed chemical recycling scheme of thiol-ene click and ROP cascade reactions.

of alkenyl and aromatic groups were not observed, indicating elimination of dechlorination proceeded simultaneously with the sulfhydryl addition reaction, and aromatic hybridization of the PVC backbone did not happen. In addition, Fourier Transform Infrared Spectroscopy (FTIR) analysis corroborates these findings, confirming the successful incorporation of sulfur sites (Supplementary Fig. 2). A substantial increase in average molecular weight was observed via gel permeation chromatography (GPC) analysis, with the molecular weight rising from the initial unreacted PVC ($M_n = 76 \text{ kg mol}^{-1}$) to 160 kg mol^{-1} . This increase is likely due to the side-chain extension on PVC through continuous ROP of LA after sulfur chlorine substitution (Fig. 2d, e). The polydispersity index (PDI) initially increased, indicating that poly lipoic acid (pLA) oligomers are produced from LA concurrently with dechlorination, and then decreased as polymerization and crosslinking advanced.

The potential mechanisms underlying the observed reaction are discussed in more detail below. Firstly, C-Cl bonds are thermally activated, and the chloride anion (Cl^-) is probably cleaved from the PVC, resulting in the formation of conjugated olefins and the release of HCl via a β -elimination mechanism. Simultaneously, disulfide bonds undergo cleavage, producing terminal sulfur radicals. The liberated HCl is subsequently neutralized by Fe ions through an electron transfer process. (Fig. 2f i–iii)²⁵. Revolving around the alternation between terminal sulfur radicals propagation and the chain transfer across the ene group, relatively weak $\text{C}=\text{C}$ π bonds are replaced with stronger C-S σ bonds, and disulfide bond networks are formed through click and ROP reactions (Fig. 2f-iv)²⁶. Energy distribution calculations of the transition state with MO6-2X/6-311⁺⁺ G (d, p) bases were performed to validate the thermodynamic properties of the cascade reaction²⁷. Supplementary Fig. 3 shows the free energetics of the transition state along the reactions on the same relative scale with starting C-Cl bonds

breaking taken as 0.0 kcal/mol. The Gibbs free energy of the overall reaction is -43.96 kcal/mol , indicating an exothermic reaction that is shown to be experimentally successful.

Efficient dechlorination and dynamic crosslinks

The solid product of the reaction is defined as DeP-x vitrimer, wherein x represents the residence time. Component-related designations, such as DeP-LA₁FeS_{0.05}, indicate the LA and FeS ratio to PVC. Notably, the principal product of our proposed strategy is the vitrimer which can be obtained by washing and drying with a final yield of >90% (Supplementary Fig. 4). As shown in Fig. 3a and Supplementary Fig. 5, the broad signal peak of DeP-12 h vitrimer at 610 cm^{-1} that belongs to the C-Cl group disappears, and the deconvoluted area ratio of the C-Cl characteristic peak decreases to 6.75%, indicating a nearly complete chlorine extraction from the PVC as residence time increase to 12 h. The deconvoluted area ratio of the C-S bond characteristic peak relative to the S-S bond decreased from 0.706 to 0.505 during the thermal recycling process, indicating an increase in the formation of S-S bonds. Due to the removal of the unstable Cl atom, the biggest weight loss (64.31 wt%) at 310°C corresponding to the release of HCl and benzene, and its derivatives disappears, as shown in thermal thermogravimetry (TG) and differential thermogravimetry (DTG) curves (Fig. 3b and Supplementary Fig. 6).

The dechlorination efficiency (De), defined as the rate of Cl atom removal, serves as a critical indicator of the successful execution of the reaction. Ion chromatography and Gas Chromatography-Mass Spectrometer (GC-MS) were performed to detect the composition of liquid by-products. Only 0.61% organic Cl (approximately 289 mg per kg of PVC) is generated in the form of nontoxic chloroalkane with 10 C atoms, as shown in the GC-MS of liquid residues (Supplementary Fig. 7). Via energy-dispersive X-ray spectroscopy (EDS) and X-ray photoelectron

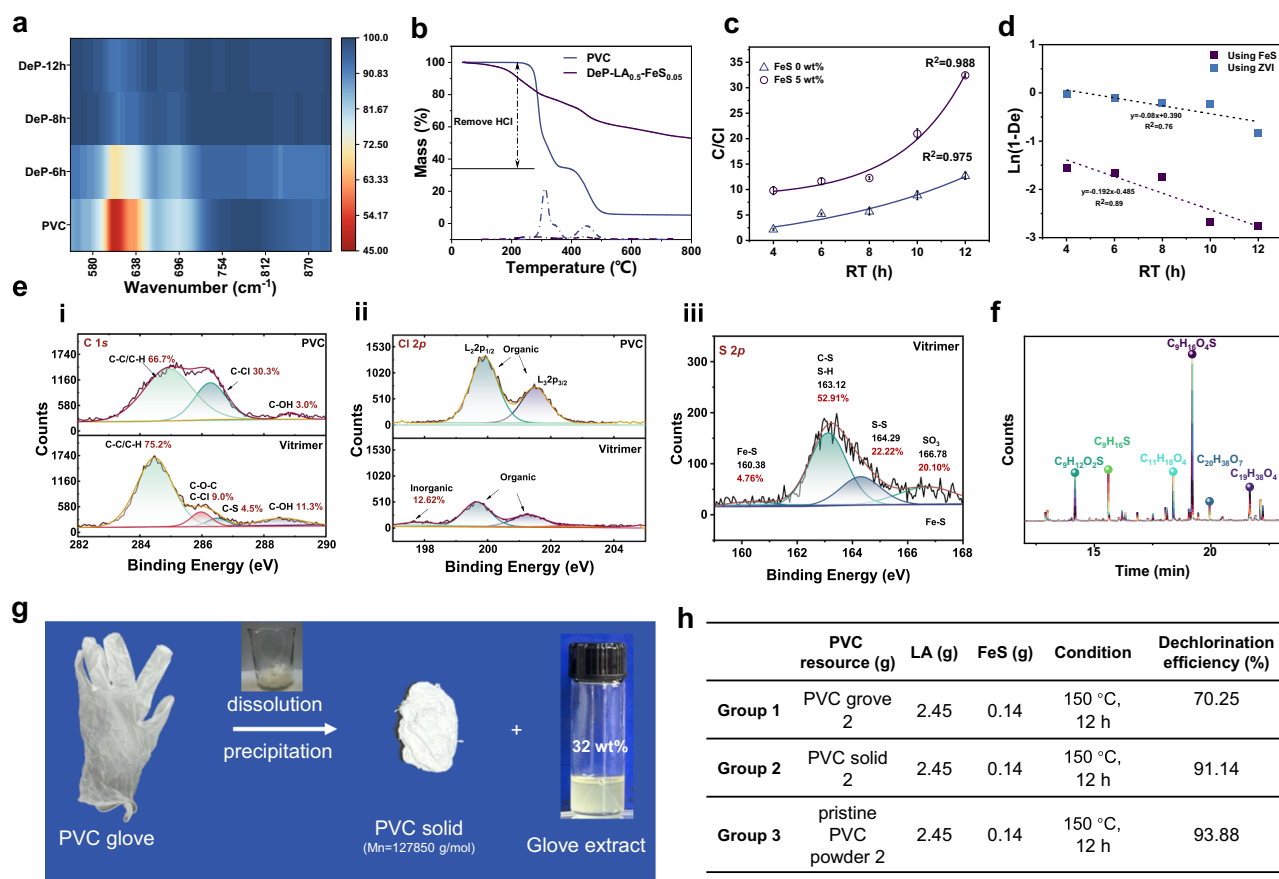


Fig. 3 | Evaluation of PVC dechlorination. **a** Heat mappings of C-Cl bond regions identified by FTIR. **b** TG, and DTG curves of PVC and vitrimer. **c** Correlations between the C/Cl ratio and residence time, three measurements were conducted for each data point with the error bars corresponding to the standard deviation. **d** First-order dechlorination kinetic fitting lines. **e** XPS analysis of dechlorination

process i, C 1s, ii, Cl 2p, and iii, S 2p spectrum, the color-filled portion indicates the peak integration area. **f** TGA-FTIR-GC/MS of decomposition products. **g** Pre-separation of plasticizer from waste PVC gloves. **h** Comparison of dechlorination efficiency using PVC gloves versus pristine PVC powder as chlorination substrates.

spectroscopy (XPS) characteristics, the residual chlorine contents and atomic bonding states in DeP vitrimer were determined. With the addition of 5 wt% FeS and lipoic acid at an S/Cl molar ratio of 1, the carbon-to-chlorine (C/Cl) ratio reaches 32.4 after a 12 h reaction (Fig. 3c), compared to 1.34 in pristine PVC and 12.66 in DeP vitrimer without FeS. This indicates that FeS nanoparticles effectively accelerate PVC dechlorination due to their high reductive activation²⁸. The dechlorination efficiency of DeP-LA₁FeS_{0.05} is 93.88%. In contrast, using non-sulfidated zerovalent iron (ZVI) particles results in a markedly lower dechlorination efficiency of 56.12% (Supplementary Fig. 8). The first-order fitting plot of dechlorination efficiency versus residence time illustrates the dechlorination kinetics. Notably, the first-order dechlorination kinetic constant is enhanced by a factor of 2.4 when FeS is employed (Fig. 3d).

As shown in Fig. 3e and Supplementary Tables 1 and 2, the C 1s XPS spectra of PVC display two dominant components: C-C/C-H at 284.99 eV and C-Cl at 286.32 eV, with peak area proportions of 66.7% and 30.3%, respectively. After dechlorination, the C-C/C-H proportion increases to 75.2%, while the C-Cl decreases to 9%²⁹. A new peak appears at a binding energy of 286.5 eV, with a peak area proportion of 4.5%, attributed to C-S functional groups (Fig. 3e-i). In addition, 12.62% of the residual Cl is present in an inorganic state (Fig. 3e-ii). The presence of distinct C-S (163.12 eV) and S-S (164.29 eV) bonding peaks in the S 2p XPS spectrum confirms the successful incorporation of sulfur into the carbon framework. A broad peak fitted at 160.38 ± 0.2 eV corresponds to sulfide (S^{2-}) or polysulfide (S_n^{2-}) species (Fig. 3e-iii)^{30,31}. We further employed TGA-FTIR-GC/MS to evaluate the degradation behavior of the vitrimers, as

shown in Fig. 3f, Supplementary Figs. 9, 10. A characteristic stretch vibration peak of $-CH_2-$ was observed at 1298 cm^{-1} within the temperature range of $180\text{--}320 \text{ }^\circ\text{C}$. Linear short-chain alkanes, primarily terminated by thiol and ketone groups, were identified in the complex gas mixture. Notably, no Cl-containing organic compounds were detected, suggesting that degradation is largely due to the thermal cleavage of weak S-S bonds, confirming the successful formation of dynamic S-S bond topology networks. These findings indicate that the proposed strategy effectively removes organic Cl, while simultaneously generating a vitrimer cross-linked via disulfide bonds.

Furthermore, we used disposable PVC gloves, commonly found in the medical, food, and electronics industries, to evaluate whether our approach can be applied to PVC waste. The gloves contain 32% liquid additives by mass, identified as di-2-ethylhexyl phthalate (DEHP) via ^1H NMR spectroscopic analysis (Supplementary Fig. 11). After the plasticizer removal (Fig. 3g), the resulting solid material (PVC solid) had an M_n of $127850 \text{ g mol}^{-1}$ and was partially soluble in DMC, as shown in GPC analysis in Supplementary Fig. 12. A 91.14% dechlorination efficiency was achieved with the PVC solid (group 2), similar to the 93.88% observed with pristine PVC powder ($M_n = 75968 \text{ g mol}^{-1}$). When using the PVC glove directly (group 1), the dechlorination rate decreased to 70.25% (Fig. 3h and Supplementary Fig. 13). These findings suggest that commercial PVC waste can be directly dechlorinated and recycled using our method. A pre-treatment involving plasticizer removal via a straightforward dissolution-precipitation method before implementing the sulfur-chlorine substitution strategy significantly improves the efficiency of dechlorination.

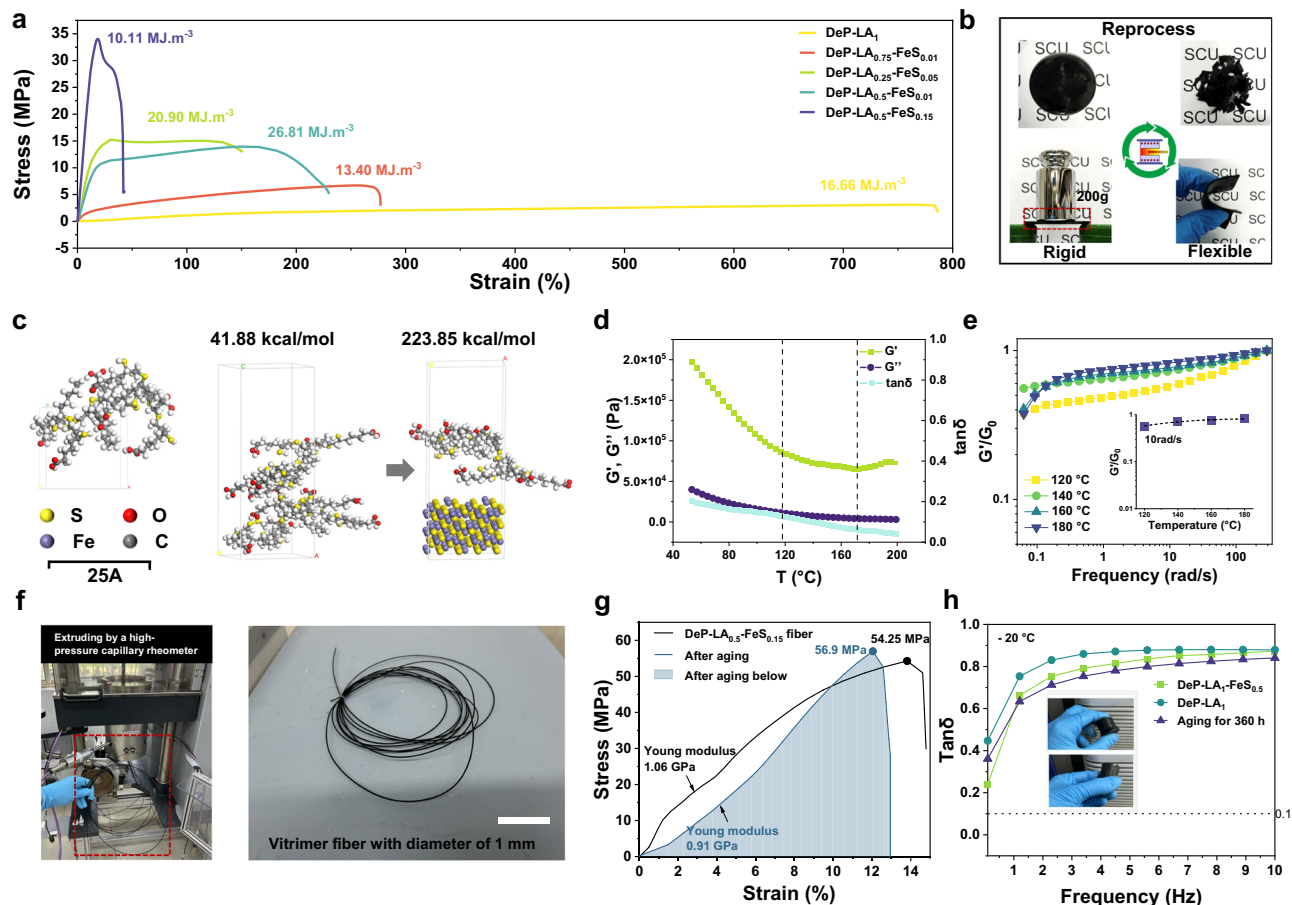


Fig. 4 | Mechanical and reprocessing properties of PVC-based vitrimers. **a** Mechanical test of vitrimers with different crosslinking structures. **b** The vitrimer reprocessing by hot pressing. **c** Schematic diagrams of MD simulations. **d** Temperature sweep of the vitrimer, the heating rate was $3\text{ }^{\circ}\text{C min}^{-1}$ ($\omega = 10\text{ rad s}^{-1}$, $\gamma = 1\%$). The shear storage (G') and loss moduli (G'') decrease at the first temperature increase stage ($45\text{--}120\text{ }^{\circ}\text{C}$), keep in a plateau ($120\text{--}165\text{ }^{\circ}\text{C}$), and increase slightly ($> 165\text{ }^{\circ}\text{C}$). **e** G'/G_0 curves of $\text{DeP-LA}_1\text{FeS}_{0.15}$

vitrimer as a function of frequency at different temperatures. **f** The digital photograph of the high-pressure spinning process and the reprocessed $\text{DeP-LA}_{0.5}\text{FeS}_{0.15}$ vitrimer fibers, scale bar 20 mm. **g** Stress-strain curves of the $\text{DeP-LA}_{0.5}\text{FeS}_{0.15}$ fibers before and after 360 h of the accelerated aging test, the color-filled portion represents the integration area of peaks. **h** The change in $\tan\delta$ with dynamic frequency ranging from 0.1 to 10 Hz, the inset pictures depict the columnar vitrimer.

Upgrading the waste PVC to value-added vitrimer

We noticed that PVC-based vitrimer exhibits unusual mechanical tunability, spanning from soft to stiff. As summarized in Fig. 4a, Supplementary Figs. 14, 15, and Table 3, the modulus varies from 1.19 to 266.3 MPa, while the elongation decreases from 784% to 40%, corresponding to variations in the content of LA and FeS nanoparticles. The mechanical performance is comparable to commercial thermosetting/thermoplastic polyolefin materials, some thermosetting resins, and rubbers (Supplementary Table 4). Under consecutive loading-unloading mechanical cycles, the soft vitrimer exhibits energy dissipation due to the dynamic network reconstruction. The topological transition temperature (T_t) of the $\text{DeP-LA}_1\text{FeS}_{0.05}$ vitrimer is determined to be $92.36\text{ }^{\circ}\text{C}$, enabling repeated recycling without a decrease in mechanical properties through hot press procedures at $140\text{ }^{\circ}\text{C}$ (Fig. 4b and Supplementary Figs. 16, 17)^{14,32}.

The encouraging mechanical performance steers a deeper investigation into the relationship between hierarchical structural characteristics and properties. In the aggregation-state structure scale, atomic force microscopy (AFM) and dark-field TEM images showed the spherical particles with diameters 80–200 nm (Supplementary Fig. 18). After dechlorination, 22.42 wt% of the initially added Fe element was retained in the vitrimer (Supplementary Fig. 19). In the valence bond scale, the presence of both bidentate coordinates and tridentate coordinates between $\text{Fe}^{2+}/\text{Fe}^{3+}$ and $-\text{COO}^-$ was revealed by XPS analysis

(Supplementary Fig. 20a and Table 2). Molecular dynamics (MD) simulations were carried out to understand the molecular origins of the mechanical advantages^{33,34}, where interfacial cohesive energy between Fe and carboxylates ($-\text{COO}^-$) of pLA was discussed. The equilibrated vitrimer models loaded FeS unit cells were shown in Fig. 4c, the binding energy is improved from 41.88 to 223.85 kcal/mol, indicating that higher mechanical force is needed for network rupture (Supplementary Figs. 20b, 21). The hardening effect of Fe ions leads to the elasticity of the network being compromised, which is consistent with the experimental studies. Considering the difference in S-S crosslinking densities, their contribution has been further discussed (Supplementary Fig. 22). Deriving from the hierarchical structures composed of the nanostructure, topology network, and metal coordination bonds, the vitrimers are endowed with exceptional tunability of strength, elasticity, and hardness.

Arising from interlaced multiple dynamic interactions, the network is adaptive to temperatures via disulfide bond exchange and supramolecular dissociation-reconstruction^{35–38}. As shown in dynamic rheological tests (Fig. 4d), the sol-gel transition doesn't occur as the G' values are higher than the G'' values over ($40\text{--}200\text{ }^{\circ}\text{C}$)³⁹. To get further insight into microstructural evolution within the adaptive networks, we adopted the Maxwell model of viscoelasticity and transient network theory to normalize the frequency-sweep rheological curves by introducing the plateau modulus $G_0(T)$ and the frequency dependence

ω , T) factor (Supplementary Figs. 23, 24)^{40,41}. The vitrimer presents non-Maxwellian behavior, which may be attributed to extra intricate polymer-nanoparticle interactions^{40,42,43}. The loss factor $\tan\delta$ (defined as G''/G') decrease pertains to an enthalpy-dominated thermodynamic behavior, as a direct consequence of bridging polymer chains detachment on the adjacent FeS nanoparticles and dynamic bond disassociation. The subsequent increase belongs to mild entropy-driven thermodynamics, where the interfacial interactions become strong as temperature increases. It is evidenced by the tiny increase of $G'/G_0(T)$ values at 10 rad/s, and the leftward shifts of the frequency-dependent rheology curve (Fig. 4e)⁴⁴. As to the analysis above, the intrinsic relation of readily tuned networks and the mechanical properties while maintaining valuable dynamic properties has been revealed. The above results give confidence that the click chemistry strategy can further introduce convenient structure regulation for PVC chemical recycling.

To evaluate the potential application of the vitrimers, we applied the high-pressure capillary rheometer to re-extrude rigid vitrimer into high-value fibers at 140 °C under 300 Pa. The tensile strength of recyclable vitrimer fiber is 54.25 MPa (Fig. 4f, g). The soft vitrimers could serve as energy-dissipation elastomers with a $\tan\delta$ value higher than 0.1 (equivalent damping ratio 10%) across a frequency range of 0.1–10 Hz, meeting ISO 22762 standards for seismic isolation bearings (Fig. 4h)⁴⁵. Furthermore, they exhibit a high $\tan\delta$ value (above 0.3) over a wide temperature range from –50 °C to over 58 °C, covering both subzero and ambient temperature conditions (Supplementary Fig. 25). Both of them show excellent aging resistance due to the removal of unstable Cl atoms. Overall, the vitrimers upcycling from waste PVC show value-added applications varying from high-performance fibers to low-temperature high-damping materials, demonstrating versatility in applications such as in the medical, buildings, and transportation fields.

Chlorine footprint and environmental risks evaluation

The environmental risks of PVC dechlorination recycling are analyzed, focusing on the emission of contamination of halogenated compounds. Statistics reveal that for every 1 kg of PVC recycled, 0.394 kg of organic chlorine is converted into inorganic chlorine, with 0.391 kg released into the liquid residue as monovalent and hypervalent ions. In addition, alkane chlorine emissions are measured at approximately 289 mg per kg of PVC, as shown in Fig. 5a. Compared with other reported treatment methods for waste PVC, such as pyrolysis and chemical recycling, our approach results in the lowest emissions of chlorinated aromatics and corrosive HCl, while also operating under a relatively moderate reaction temperature, as summarized in Fig. 5b and Supplementary Table 5.

As depicted in Fig. 5c, pyrolysis tars predominantly consist of aromatic compounds, including chlorobenzene, polychlorinated benzenes, and dioxin byproducts. In contrast, only small amounts of liquid alkane paraffin are produced during our one-step dechlorination reaction because of minimal chain scission and decomposition. Alcohols, aldehydes, and acids compounds containing 4–22 carbon atoms were identified through GC-MS analysis, as presented in Supplementary Fig. 26. We carried out the USEtox, recommended as the best evaluation tool for the life cycle environmental performance of products^{6,46,47}, to assess the human toxicological and ecotoxicological impacts of the chemical emissions deriving from the recycling of PVC. This process involves calculating a weighted sum of the releases of various compounds by utilizing characterization factors:

$$IS = \sum_i \sum_x CF_{x,i} * m_{x,j} \quad (1)$$

In this equation, IS represents the impact score, $CF_{x,i}$ denotes the characterization factor of substance x emitted to compartment i , and

$m_{x,i}$ indicates the mass of substance x released into compartment i (kg). Human toxicity is defined as the cumulative cases of cancer or non-cancer health effects per kilogram of contaminants released into different environments, including household indoor air, occupational indoor air, urban air, continental rural air, continental (coastal) seawater, continental agricultural soil and/or continental natural soil. The metric used for this assessment is expressed in terms of Disability-Adjusted Life Years (DALY) at the endpoint level per kilogram emission (DALY/kg_{emitted}⁻¹). The unit of the characterization factor for ecosystem toxicity is potentially affected fraction of species (PAF) at the midpoint level integrated over the freshwater volume (m³) and 1 day (d) per kg emission, PAF·m³·d·kg_{emitted}⁻¹ (details in Supplementary methods). Chlorinated aromatic compounds, derived from pyrolysis recycling and recognized as major contributors to toxic pollution, were included as counterparts in our analysis. Characterization factors for these compounds, summarized as comparative toxic units for human toxicity (CTU_h, Supplementary Figs. 27–30 and Tables 6, 7), were sourced from the USEtox database⁴⁶. As shown in Fig. 5d, under equivalent emission conditions, the total IS value of the primary alkane byproducts in this work is 3.11*10⁻⁵ across all emission scenes, which is significantly lower than 7.78*10⁻³ for the principal pyrolysis byproducts—representing only 0.43% of their toxic potential. Additionally, in the freshwater ecosystem, the most impacted scenario, our strategy reduces the IS by 99.6% (Fig. 5e). In the seawater scenario, the least affected, ecosystem toxicity dramatically decreases from 681 to 0.077 PAF·m³·d. Overall, the total ecosystem toxicity risks are also reduced to 0.49% of counterparts. In brief, owing to near-zero emission of organochlorine contaminant, the proposed strategy enabled by a coupling of thiol-ene click and dynamic polymerization efficiently mitigates negative impacts in terms of ecotoxicity, human exposure, and health concerns, offering a sustainable alternative for waste PVC treatment.

Discussion

To sum up, this work pioneers a concept of backbone protective dechlorination towards PVC upcycling, leveraging cascade thiol-ene click and reversible ROP reaction to achieve precise sulfur-chlorine substitution and in situ dynamic crosslinks. Notably, dechlorinated PVC is upcycled into robust, recyclable cross-linked vitrimer. Efficient Cl removal and inorganicization mitigate the ecotoxicity, human exposure, and health risks associated with waste PVC recycling. The strategy is foreseen to address the challenges in harmless and high-valuable circulation regeneration of various currently halogen-containing hazardous plastics. Most importantly, this work motivates a rethinking of dynamic bond effects in one-step chemical recycling, wherein they are intentionally designed to facilitate a future recycling process at the macromolecular level.

Methods

Reagents and materials

Raw PVC powder (sieved through a 100 mesh, $M_n = 75968$ g/mol) with a chlorine content of 42.06 wt% was purchased from Hongxing Polymer Co., Ltd. Dimethyl carbonate (DMC, AR, 98%), lipoic acid (LA, 99%), and 5,5-dimethyl-pyrroline N-oxide (DMPO, 97 + %) were purchased from Sigma-Aldrich (USA). The Sodium dithionite (Na₂S₂O₄, 80 + %), Ferric chloride (FeCl₃·6H₂O, 98 + %), zero-valent iron (ZVI, 99.5%), tetrahydrofuran (THF, 99.9%), THF-d₈ and sodium borohydride (NaBH₄, 98 + %) were supplied by Shanghai Maikelin Biochemical Technology Co., Ltd. Disposable PVC gloves (Ammex) were purchased from Jiangsu Jiesheng Co., Ltd. All reagents and ingredients were used without further purification. Deionized water (resistivity: 18.3 MΩ cm) was used for all the experiments.

FeS nanoparticles preparation

FeS nanoparticles were prepared according to the following procedure. Briefly, sodium dithionite (2.0 g) was dissolved in 1 L of 0.8 M

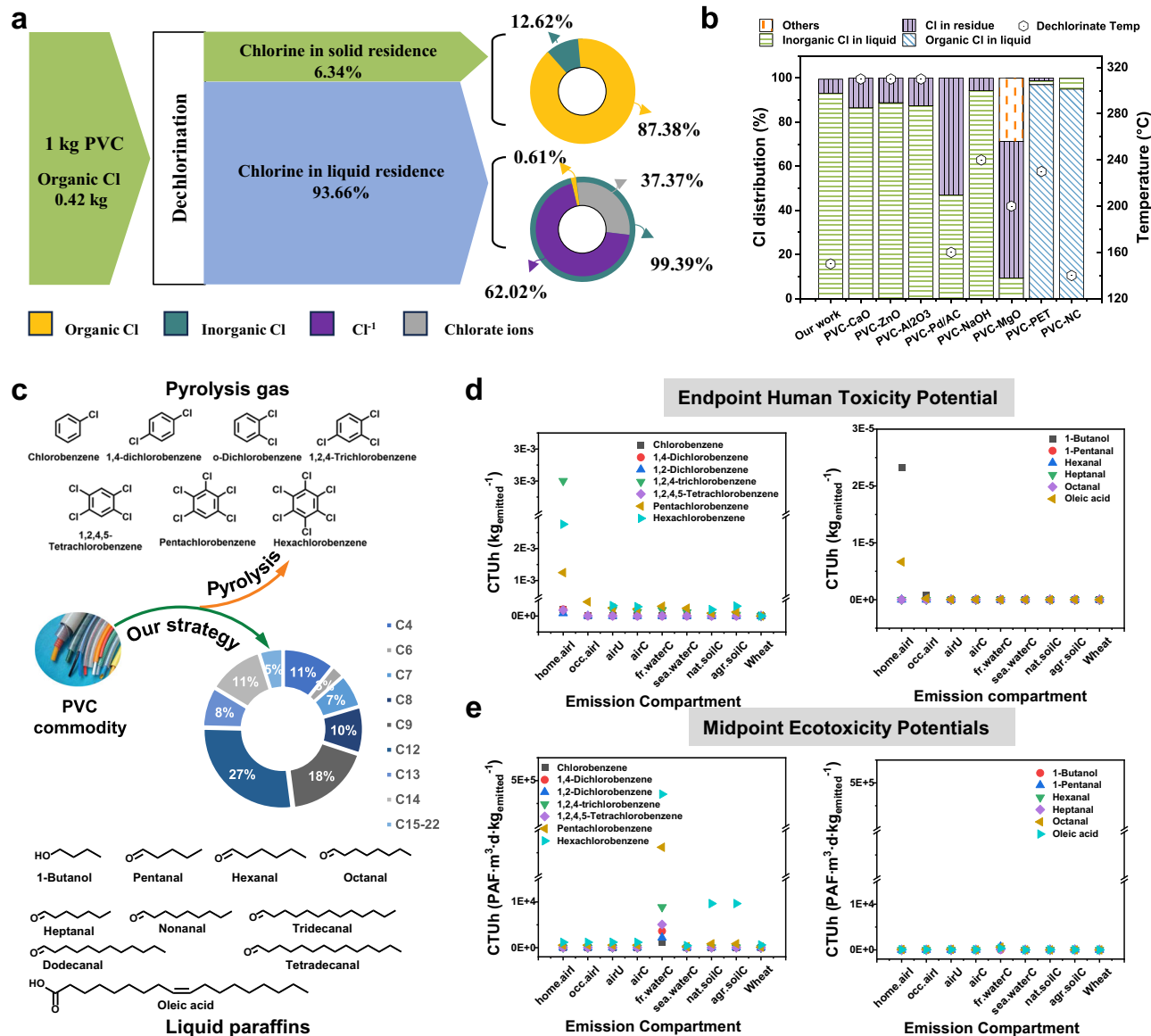


Fig. 5 | Chlorine element footprint evaluation for environmental impact.

a Statistics on chlorine element flow. **b** A comparison of chlorine distribution between high-temperature pyrolysis and chemical recycling methods^{13,14,51–54}. **c** Comparison of main by-product composition formed in a PVC pyrolysis reaction⁵⁵

NaBH₄. The resulting solution was then added dropwise to 0.5 M FeCl₃ in a 3:1 volume ratio. The solution was decanted, and the precipitates were rinsed with degassed water several times. The ultrapure water was degassed with high-purity N₂ for 30 min. The particles were dried in a vacuum oven for 1 d and stored in an anaerobic chamber before use and characterization.

One-step dechlorination upcycling reaction of waste PVC

The hydrothermal dechlorination experiments were carried out in a 50 mL autoclave. A mixture of 5 g of PVC, 6.125 g of LA, 0.35 g of FeS, and 20 mL of DMC was loaded into airtight stainless-steel tubular reactors with internal Teflon containers. The FeS-to-PVC mass ratio varied from 1% to 15% to study the dechlorination rate, while the S/Cl atom ratio ranged from 10% to 100%. The temperature was increased in two stages, initially at 80 °C for 30 min, followed by a rise to 150 °C with residence times of 4, 6, 8, 10, and 12 h to assess chlorine removal efficiency. After the reaction, the system was cooled, and depressurized, and the products were separated into solid and

liquid phases via filtration. The solid phase was washed, dried at 65 ± 5 °C until no weight loss, and labeled as DeP-LAXFeSy, with x and y indicating the LA and FeS proportions, respectively. The reactor's inner Teflon surface was rinsed with DMC and water, and all washing solutions were collected for chlorine distribution analysis. Experiments were performed in triplicate to ensure consistency, and the average values were reported.

A discarded glove (2 g) was cut into small pieces (~0.5 cm) and dissolved in 50 mL of THF at room temperature (~30 min). The polymer was precipitated in 200 mL of cold methanol with stirring, collected by filtration, and the filtrate was concentrated under reduced pressure to yield PVC_{solid}. This dissolution-precipitation process was repeated twice more. The combined filtrates were concentrated and dried under vacuum overnight, yielding 0.642 g of a colorless plasticizer (32% relative to glove mass). We then applied the same hydrothermal procedure to recycle the disposable PVC gloves and the PVC_{solid}, which had already undergone plasticizer removal.

The solid phase was washed, dried at 65 ± 5 °C until no weight loss, and labeled as DeP-LAXFeSy, with x and y indicating the LA and FeS proportions, respectively. The reactor's inner Teflon surface was rinsed with DMC and water, and all washing solutions were collected for chlorine distribution analysis. Experiments were performed in triplicate to ensure consistency, and the average values were reported.

Dechlorination reaction process characterization

Electron paramagnetic resonance (EPR) spectroscopy measurements were conducted by using an EMXplus spectrometer (BRUKER, Germany) equipped with the temperature control systems and High Sensitivity Probe-Head (Bruker) in a small quartz flat cell (Wilma-LabGlass, WG 808-Q). 0.5 mL DMPO of DMC solution was used as a spin-trapping reagent. The samples (ca 200 mg) were flame-sealed in quartz tubes under reduced air pressure (ca 500 torr). The measurement was carried out by placing the unreacted compounds in the cavity of the EPR spectrometer and heating the samples to 140 °C from 25 °C^{48,49}. The ROP and thiol-ene click reactions happened while concomitant continuous records of the EPR spectra. The experimental conditions were as follows: Microwave Frequency = 9.8 GHz, Microwave Power = 0.5024 mW, Modulation Amplitude = 1.0 G, and Sweep Time = 30 s²³. FTIR analysis of the solid products under different residence times was performed on a Nicolet iS50 Fourier transform spectrometer (USA) in ATR mode. The HCl loss could be monitored by the TG209F1 (NETZSCH, Germany) from 25 to 800 °C at a heating rate of 20 °C min⁻¹ in the N₂ atmosphere to investigate the time influence on the dechlorination process. Qualitative and quantitative analysis of liquid phase products was performed by gas chromatography (GC-MS, GCMS-QP2010 Plus, Japan) equipped with a hydrogen flame-ionization detector (FID), electron ionization mass detector (EI-MS), and HP-5 nonpolar column. The GC yield was determined based on internal standard curves and integrated peak areas. Determination of the molecular weight and polydispersity of the vitrimer was performed using Gel Permeation Chromatography (GPC, Waters 1515, US), equipped with a refractive index detector (RI), and Dual-Angle Light Scattering detector. THF was used as an eluent. For the measurement after the reaction, the organic components were dissolved in THF (2 mg/mL)¹. ¹H, and ¹³C NMR spectra were recorded on a Bruker Avance III HD 400 MHz instrument. The reaction mixture (10 mg) was diluted with THF-d₈ (0.6 mL) and directly used for ¹H NMR experiment.

Quantitative analysis of Cl element distribution

Both the chlorine content of DeP-LA_xFeS_y and filtrate were measured. The residual chlorine content in solid upcycled products can be measured using SEM energy-dispersive X-ray spectroscopy mapping (JEOL JSM-5900LV, Japan). The relative chlorine contents in filtrate can then be accurately determined using the ion chromatography technique (CIC-DI60, China). According to the data, the degree of dechlorination of PVC is defined as Eq. (2):

$$De(\%) = \left(1 - \frac{C_{\text{solid product}}^{\text{Cl}} * m_{\text{solid product}}}{C_{\text{raw PVC}}^{\text{Cl}} * m_{\text{raw PVC}}} \right) * 100\% \quad (2)$$

where De is dechlorination efficiency, $C_{\text{solid product}}^{\text{Cl}}$ and $C_{\text{raw PVC}}^{\text{Cl}}$ denote the concentrations of the organic chlorine in the solid product and raw PVC, respectively, and $m_{\text{solid product}}$ and $m_{\text{raw PVC}}$ denote the masses of the solid product and raw PVC, respectively.

According to the law of mass action, the chemical reaction rate is related to the concentration of the reactants and can be written as Eq. (3):

$$\frac{dX}{dt} = -kX^n \quad (3)$$

where X was the mass fraction calculated by dividing the mass of chlorine in the solid product by the mass of chlorine in PVC, 100-De, %; τ was the residence time, h; k was the chemical reaction rate constant, h⁻¹. First-order reaction assumption to calculate the dechlorination kinetic parameters of PVC and achieved satisfactory calculation accuracy. For $n=1$, the Eq. (3) can be

integrated into Eq. (4):

$$\ln(1 - De) = -k\tau \quad (4)$$

Rheological and reprocessing characterization of vitrimers

The obtained columnar solid products DeP-LA_xFeS_y were subjected to compression molding at 140 °C and 15 MPa for the optimum time (10 min) to produce the sheet vitrimer. The vitrimer was cut into small pieces and then compression molded under the same procedure. The samples were left to stand under ambient conditions for 24 hours before measurements. Thermodynamic properties were evaluated using a TA Instrument (DMA Q800, USA) in tension mode. Rectangular samples (gauge length: 20 mm, width: 2 mm, thickness: 0.5 mm) were used in all tests unless specified otherwise. The samples were heated from -50 °C to 160 °C at a rate of 5 °C/min, with the frequency set at 1 Hz and strain at 0.1%. A frequency sweep mode was applied in the range of 0.1–10 Hz, while the temperature was maintained at -20 °C. The dynamic rheological tests were performed on ThermoFisher, HAAKE MARS 60, (USA) to assess the viscoelastic properties of vitrimers. To prepare the samples for rheology, the samples were placed into a mold and hot pressed at 140 °C for 10 min to ensure uniformity, and then cut to a standard round shape with a diameter of 8 mm. Tests were conducted using 8 mm stainless steel parallel plates with a forced convection oven accessory for controlling temperature above ambient. Cool nitrogen gas from liquid nitrogen was blown through the convection oven to access sub-ambient temperatures. For the frequency sweep test, the experiments were conducted with an angular frequency range from 6*10⁻² to 3*10² rad/s at a variety of temperatures ranging from 120 to 180 °C. For the temperature sweep, the experiments were conducted from 45 to 200 °C with a frequency of 10 rad/s. Since most of the measurement was conducted in the rubbery plateau regime, the strain amplitude during the measurement was chosen to be 1%. The Maxwell model of viscoelasticity predicts a single relaxation time, τ_m , that can be determined from the crossover frequency as Eqs. 5–8, where ω_m is the frequency defined at the crossover of the storage modulus G' and loss modulus G'' . This equation is dimensionless with $G''^* = G_0(T)/2$ since the maximum occurs at a frequency of $1/\tau_m$. The Maxwell relationship can be written to eliminate frequency dependence as Eqs. (5–8)⁴⁰:

$$G' = \frac{G_0(T)(\omega\tau_m)^2}{1 + (\omega\tau_m)^2} \quad (5)$$

$$G'' = \frac{G_0(T)(\omega\tau_m)}{1 + (\omega\tau_m)^2} \quad (6)$$

$$\tau_m = \frac{1}{\omega_m} \quad (7)$$

$$G''^* = \frac{G_0(T)}{2\sqrt{G''^* * (2 - G''^*)}} \quad (8)$$

Vitrimer properties evaluation

Mechanical and thermal characteristics of vitrimer are of primary significance when considering the targeted reprocessing, and correlations between the structure and properties of the vitrimer should be established. The thermal decomposition behavior of the vitrimers was studied using TGA-FTIR-GC/MS (PerkinElmer, USA). Degradation products generated at the maximum degradation rate (temperature range between 280–310 °C) were synchronously detected by the GC-MS system. X-ray photoelectron spectroscopy was performed on XPS-Supra (Kratos, UK)

to determine the elemental compositions, atomic bonding states, and relatively quantitative changes of Cl elements before and after dechlorination. Mechanical properties were tested on Instron 5560 (USA) with a 1 kN load cell at a constant strain rate of 50 mm min⁻¹ under ambient conditions. All specimens were cut to standard shapes (a gauge length of 20 mm, a width of 2 mm, and a thickness of 0.5 mm) with a dumbbell knife before tests. The rigid vitrimer was re-extruded into high-performance fibers using a high-pressure capillary rheometer (RG120, Germany) under controlled conditions: 140 °C temperature, 300 Pa pressure, and a die with a 10:1 diameter ratio.

Cross-linking density was determined by an equilibrium swelling experiment based on the Flory-Rehner equation²⁴. The equilibrium swelling experiment was conducted by immersing vulcanizations in toluene at room temperature for 72 h. After swelling, the solvent was wiped off quickly from the sample surface using filter paper, and the samples were immediately weighed and then dried in a vacuum oven at 65 ± 5 °C until constant weight. The crosslinking density (V_e) is calculated according to the Eq. (9):

$$V_e = \frac{\ln(1 - V_r) + V_r + \chi V_r^2}{V_s \left(V_r^{\frac{1}{3}} - \frac{V_r}{2} \right)} \quad (9)$$

where χ is the Flory-Huggins polymer-solvent interaction parameter (near 0.34 for vitrimer and toluene), and V_s is the molar volume of the solvent (106.5 cm³/mol for toluene). V_r is the volume fraction of vitrimer in the swollen gel, which is calculated by the following Eq. (10):

$$V_r = \frac{(m_2 - m_0\phi)\rho_r}{(m_2 - m_0\phi)\rho_r + \frac{m_1 - m_2}{\rho_s}} \quad (10)$$

where m_0 is the sample mass before swelling, m_1 , and m_2 are the weights of the swollen and de-swollen vitrimer, respectively, ϕ is the weight fraction of the insoluble components (5% FeS nanoparticles), ρ_r and ρ_s are the densities of the vitrimer and solvent (0.872 g/cm³), respectively. Further details on the experimental setup and characterization can be found in Supplementary methods.

Molecular dynamic simulation

The molecular dynamic simulation was performed under a universal force field in Material Studio 2018⁵⁰. Molecular models of the vitrimer were first built and geometrically optimized based on the Forcite module. Besides, the cell of FeS was built from the experimental crystallographic data. Then, an amorphous cell loaded with one vitrimer structural unit and FeS periodic structure was constructed, then geometrical optimization procedures were carried out again to obtain the overall system with initial energy minimization. During the geometrical optimization process, the FeS crystal was constrained at the bottom of the cell. The isothermal-isochoric molecular dynamic simulation of FeS composite models was conducted at 600 K. The binding energy was calculated and compared to the final conformation models using the following Eq. (11):

$$E_{\text{binding}} = E_{\text{FeS}} + E_{\text{vitrimer}} - E_{\text{total}} \quad (11)$$

in which E_{FeS} , E_{vitrimer} represents the corresponding energy of the FeS and vitrimer in the equilibrium conformation; E_{total} and E_{binding} is the total energy and binding energy of this model. Further information on our simulations can be found in Supplementary methods.

Data availability

All data generated in this study are provided in the Supplementary Information/Source Data file or are available from the corresponding author upon request. Source data are provided in this paper.

References

- Lau, W. W. Y. et al. Evaluating scenarios toward zero plastic pollution. *Science* **369**, (2020).
- Law, K. L. & Narayan, R. Reducing environmental plastic pollution by designing polymer materials for managed end-of-life. *Nat. Rev. Mat.* **7**, 104–116 (2021).
- Li, C. et al. Nitrogen doping induced by intrinsic defects of recycled polyethylene terephthalate-derived carbon nanotubes. *SusMat* **3**, 431–440 (2023).
- MacLeod, M., Arp, H. P. H., Tekman, M. B. & Jahnke, A. The global threat from plastic pollution. *Science* **373**, 61–65 (2021).
- Borrelle, S. B. et al. Predicted growth in plastic waste exceeds efforts to mitigate plastic pollution. *Science* **369**, 1515–1518 (2020).
- Xu, S. et al. Upcycling chlorinated waste plastics. *Nat. Rev. Methods Primers* **3**, 1–19 (2023).
- Jiang, X., Zhu, B. & Zhu, M. An overview on the recycling of waste poly(vinyl chloride). *Green Chem.* **25**, 6971–7025 (2023).
- Lu, L., Li, W., Cheng, Y. & Liu, M. Chemical recycling technologies for PVC waste and PVC-containing plastic waste: A review. *Waste Manage.* **166**, 245–258 (2023).
- Liu, M., Wu, X. & Dyson, P. J. Tandem catalysis enables chlorine-containing waste as chlorination reagents. *Nat. Chem.* **16**, 700–708 (2024).
- Choi, C. et al. Efficient electrocatalytic valorization of chlorinated organic water pollutant to ethylene. *Nat. Nanotechnol.* **18**, 160–167 (2022).
- Kots, P. A., Vance, B. C., Quinn, C. M., Wang, C. & Vlachos, D. G. A two-stage strategy for upcycling chlorine-contaminated plastic waste. *Nat. Sustain.* **6**, 1258–1267 (2023).
- Fagnani, D. E., Kim, D., Camarero, S. I., Alfaro, J. F. & McNeil, A. J. Using waste poly(vinyl chloride) to synthesize chloroarenes by plasticizer-mediated electro(de)chlorination. *Nat. Chem.* **15**, 222–229 (2022).
- Cao, R. et al. Co-upcycling of polyvinyl chloride and polyesters. *Nat. Sustain.* **6**, 1685–1692 (2023).
- Christensen, P. R., Scheuermann, A. M., Loeffler, K. E. & Helms, B. A. Closed-loop recycling of plastics enabled by dynamic covalent diketoenamine bonds. *Nat. Chem.* **11**, 442–448 (2019).
- Qin, B. et al. Closed-loop chemical recycling of cross-linked polymeric materials based on reversible amidation chemistry. *Nat. Commun.* **13**, 7595 (2022).
- Zhang, S. et al. Depolymerization of polyesters by a binuclear catalyst for plastic recycling. *Nat. Sustain.* **6**, 965–973 (2023).
- Lou, X. et al. Grave-to-cradle photothermal upcycling of waste polyesters over spent LiCoO₂. *Nat. Commun.* **15**, 2730 (2024).
- Devaraj, N. K. & Finn, M. G. Introduction: Click chemistry. *Chem. Rev.* **121**, 6697–6698 (2021).
- Kumar, G. S. & Lin, Q. Light-triggered click chemistry. *Chem. Rev.* **121**, 6991–7031 (2021).
- Zhang, Q., Qu, D. H., Feringa, B. L. & Tian, H. Disulfide-mediated reversible polymerization toward intrinsically dynamic smart materials. *J. Am. Chem. Soc.* **144**, 2022–2033 (2022).
- Hoyle, C. E. & Bowman, C. N. Thiol-ene click chemistry. *Angew. Chem. Inter. Ed.* **49**, 1540–1573 (2010).
- Choi, H., Kim, M., Jang, J. & Hong, S. Visible-light-induced cysteine-specific bioconjugation: biocompatible thiol-ene click chemistry. *Angew. Chem. Inter. Ed.* **59**, 22514–22522 (2020).
- Tian, C. et al. Accelerated degradation of microplastics at the liquid interface of ice crystals in frozen aqueous solutions. *Angew. Chem. Inter. Ed.* **61**, e202206947 (2022).
- Wang, D., Tang, Z., Liu, Y. & Guo, B. Crosslinking diene rubbers by using an inverse vulcanised co-polymer. *Green Chem.* **22**, 7337–7342 (2020).
- Bang, E.-K. et al. Substrate-initiated synthesis of cell-penetrating poly(disulfide)s. *J. Am. Chem. Soc.* **135**, 2088–2091 (2013).

26. Northrop, B. H. & Coffey, R. N. Thiol-ene click chemistry: Computational and kinetic analysis of the influence of alkene functionality. *J. Am. Chem. Soc.* **134**, 13804–13817 (2012).
27. Demarteau, J. et al. Circularity in mixed-plastic chemical recycling enabled by variable rates of polydiketoenamine hydrolysis. *Sci. Adv.* **8**, 8823 (2022).
28. Brumovský, M. et al. Core-shell Fe/Fes nanoparticles with controlled shell thickness for enhanced trichloroethylene removal. *ACS Appl. Mater. Interfaces* **12**, 35424–35434 (2020).
29. Ma, D. et al. Dechlorination of polyvinyl chloride by hydrothermal treatment with cupric ion. *Process Saf. Environ.* **146**, 108–117 (2021).
30. Srinivas, K. et al. Fe-Nx sites coupled with core-shell FeS@C nanoparticles to boost the oxygen catalysis for rechargeable Zn-air batteries. *J. Energy Chem.* **90**, 565–577 (2024).
31. Wang, X. et al. A soft multifunctional film from chitosan modified with disulfide bond cross-links and prepared by a simple method. *Int. J. Biol. Macromol.* **253**, 126774 (2023).
32. Saito, K., Eisenreich, F., Türel, T. & Tomović, Ž. Closed-loop recycling of poly(Imine-Carbonate) derived from plastic waste and bio-based resources. *Angew. Chem. Int. Ed.* **61**, e202211806 (2022).
33. Li, C. et al. Photoswitchable and reversible fluorescent eutectogels for conformational information encryption. *Angew. Chem.* **135**, e202313971 (2023).
34. Qiu, X., Yang, X., Guo, Q., Liu, J. & Zhang, X. Ln-HOF nanofiber organogels with time-resolved luminescence for programmable and reliable encryption. *Nano Lett.* **23**, 11916–11924 (2023).
35. Chakma, P. & Konkolewicz, D. Dynamic covalent bonds in polymeric materials. *Angew. Chem. Int. Ed. Engl.* **58**, 9682–9695 (2019).
36. Wu, S. & Chen, Q. Advances and new opportunities in the rheology of physically and chemically reversible polymers. *Macromolecules* **55**, 697–714 (2022).
37. Khare, E., Holten-Andersen, N. & Buehler, M. J. Transition-metal coordinate bonds for bioinspired macromolecules with tunable mechanical properties. *Nat. Rev. Mater.* **6**, 421–436 (2021).
38. Yu, S. et al. Topological network design toward high-performance vegetable oil-based elastomers. *SusMat* **3**, 320–333 (2023).
39. Chen, C. et al. Tannic acid-thioctic acid hydrogel: a novel injectable supramolecular adhesive gel for wound healing. *Green Chem.* **23**, 1794–1804 (2021).
40. Bischoff, D. J. et al. Unraveling the rheology of inverse vulcanized polymers. *Nat. Commun.* **14**, 7553 (2023).
41. Tanaka, F. & Edwards, S. F. Viscoelastic properties of physically crosslinked networks: Part 2. Dynamic mechanical moduli. *J. Non-newton. Fluid Mech.* **43**, 273–288 (1992).
42. Su, Y. et al. High-entropy microdomain interlocking polymer electrolytes for advanced all-solid-state battery chemistries. *Adv. Mater.* **35**, 2209402 (2023).
43. Cui, Y. et al. A perspective on high-entropy two-dimensional materials. *SusMat* **2**, 65–75 (2022).
44. Yu, A. C. et al. Physical networks from entropy-driven non-covalent interactions. *Nat. Commun.* **12**, 746 (2021).
45. Zhao, J., Jiang, N., Zhang, D., He, B. & Chen, X. Study on optimization of damping performance and damping temperature range of silicone rubber by polyborosiloxane gel. *Polymers* **12**, 1196 (2020).
46. Rosenbaum, R. K. et al. USEtox - The UNEP-SETAC toxicity model: Recommended characterisation factors for human toxicity and freshwater ecotoxicity in life cycle impact assessment. *Inter. J. Life Cycle Assess.* **13**, 532–546 (2008).
47. Fantke, P. et al. Exposure and toxicity characterization of chemical emissions and chemicals in products: global recommendations and implementation in USEtox. *Inter. J. Life Cycle Assess.* **26**, 899–915 (2021).
48. Yang, Y. et al. Self-strengthening, self-welding, shape memory, and recyclable polybutadiene-based material driven by dual-dynamic units. *ACS. Appl. Mater. Interfaces* **14**, 3344–3355 (2022).
49. Elian, C., Brezová, V., Sautrot-Ba, P., Breza, M. & Versace, D. L. Lawsons derivatives as efficient photopolymerizable initiators for free-radical, cationic photopolymerizations, and thiol-ene reactions. *Polymers* **13**, 2015 (2021).
50. Wang, N., Yang, X. & Zhang, X. Ultrarobust subzero healable materials enabled by polyphenol nano-assemblies. *Nat. Commun.* **14**, 814 (2023).
51. Meng, T. T., Zhang, H., Lü, F., Shao, L. M. & He, P. J. Comparing the effects of different metal oxides on low temperature decomposition of PVC. *J. Anal. Appl. Pyrolysis* **159**, 105312 (2021).
52. Nishibata, H., Uddin, M. A. & Kato, Y. Simultaneous degradation and dechlorination of poly(vinyl chloride) by a combination of superheated steam and CaO catalyst/adsorbent. *Polym. Degrad. Stab.* **179**, 109225 (2020).
53. Lv, B., Zhao, G., Li, D. & Liang, C. Dechlorination and oxidation for waste poly(vinylidene chloride) by hydrothermal catalytic oxidation on Pd/AC catalyst. *Polym. Degrad. Stab.* **94**, 1047–1052 (2009).
54. Li, T., Zhao, P., Lei, M. & Li, Z. Understanding hydrothermal dechlorination of PVC by focusing on the operating conditions and hydrochar characteristics. *Appl. Sci.* **7**, 256 (2017).
55. Font, R., Gálvez, A., Moltó, J., Fullana, A. & Aracil, I. Formation of polychlorinated compounds in the combustion of PVC with iron nanoparticles. *Chemosphere* **78**, 152–159 (2010).

Acknowledgements

The authors thank the National Natural Science Foundation of China (52173112, 52373116, received by X.Z.). The authors also thank Dr. Guiping Yuan from the Analytical and Testing Centre of Sichuan University for providing the TEM measurement.

Author contributions

X.Z. supervised the project and provided Funding. X.Z. and X.Q. conceived the project. X.Q. performed all experiments, and data analysis, created the figures, and wrote the original draft. J.L., X.L., and Y.W. contributed to the figure creation, revision of the paper, investigation, and formal analysis.

Competing interests

The authors declare no competing interests.

Additional information

Supplementary information The online version contains supplementary material available at <https://doi.org/10.1038/s41467-024-53984-x>.

Correspondence and requests for materials should be addressed to Xinxing Zhang.

Peer review information *Nature Communications* thanks the anonymous reviewers for their contribution to the peer review of this work. A peer review file is available

Reprints and permissions information is available at <http://www.nature.com/reprints>

Publisher's note Springer Nature remains neutral with regard to jurisdictional claims in published maps and institutional affiliations.

Open Access This article is licensed under a Creative Commons Attribution-NonCommercial-NoDerivatives 4.0 International License, which permits any non-commercial use, sharing, distribution and reproduction in any medium or format, as long as you give appropriate credit to the original author(s) and the source, provide a link to the Creative Commons licence, and indicate if you modified the licensed material. You do not have permission under this licence to share adapted material derived from this article or parts of it. The images or other third party material in this article are included in the article's Creative Commons licence, unless indicated otherwise in a credit line to the material. If material is not included in the article's Creative Commons licence and your intended use is not permitted by statutory regulation or exceeds the permitted use, you will need to obtain permission directly from the copyright holder. To view a copy of this licence, visit <http://creativecommons.org/licenses/by-nc-nd/4.0/>.

© The Author(s) 2024